Scintillation Crystal Design Features for a Miniature Gamma Ray Camera

Andrew P. Dhanasopon, Craig S. Levin, *Member, IEEE*, Angela M. K. Foudray, *Student Member, IEEE*, Peter D. Olcott, and Frezghi Habte, *Member, IEEE*

***Abstract*—A miniature scintillation camera with a 5 cm × 5 cm field-of-view (FOV) is being developed to aid in surgical staging of cancer. This paper reports on certain interesting design aspects of the scintillation crystal array. Simulations and measurements of different types of crystal materials revealed that lutetium oxyorthosilicate (LSO), which is ordinarily used in PET, has appealing properties for detecting 140 keV photons. For example, LSO requires only 3 mm of thickness for 95% detection efficiency at 140 keV. This small thickness is appealing for high light collection efficiency, narrow light distribution, and minimizing the LSO volume in order to reduce intrinsic background events produced by ^{176}Lu (2.6% abundance). Studies of both discrete and sheet crystals revealed that discrete crystal arrays have the advantage of increased spatial linearity and dynamic range compared to crystal sheets. For optimizing sensitivity and spatial resolution, several crystal array conditions were investigated, including ground crystal pixels packed tightly together with internal reflectors and with optical coupling grease. This design focuses the light, but also allows adequate light sharing for positioning with the position sensitive photomultiplier tube (PSPMT) that will be used in the gamma camera.**

***Index Terms*—Detectors, gamma camera, gamma ray imaging, Monte Carlo simulations, scintillation crystal, surgical staging.**

I. Introduction

DETECTION and localization of the closest, or "sentinel," lymph node to a primary tumor is important for the staging of cancer, because it avoids unnecessary dissection of the lymphatic system. Presently, ^{99m}Tc-sulfur colloid is used for the detection of the sentinel lymph nodes before surgery through lymphoscintigraphy using a standard gamma ray camera, and during surgery using a nonimaging radiation detector. Standard scintillation cameras used today for presurgical planning are typically not mobile and are too large to bring into a surgical suite [1]. For surgical staging, a small scintillation camera would be useful in certain situations in which the sentinel node cannot be located with a simple gamma radiation probe and/or blue dye.

A miniature scintillation camera is being developed with a 5 cm × 5 cm field-of-view (FOV) that will use a cerium-doped lutetium oxyorthosilicate (LSO:Ce) scintillation crystal array to aid in the surgical staging of cancer. Both simulations and experiments were performed, by investigating light collection and light distribution, in order to guide the choice of crystal material and crystal array parameters. This paper reports on the interesting design features of the LSO crystal array for the miniature gamma ray camera.

Manuscript received November 15, 2003; revised October 12, 2004. This work was supported in part by Research Grant RG-01-0492 from the Whitaker Foundation, and by the Howard Hughes Undergraduate Research Apprenticeship Program at the University of California, San Diego.

The authors are with the Departments of Bioengineering and Physics, University of California at San Diego, La Jolla, CA 92093 and also with the Department of Radiology, Stanford University School of Medicine, Stanford, CA 94305 USA (e-mail: cslevin@stanford.edu).

Digital Object Identifier 10.1109/TNS.2005.858178

II. Materials and Methods

A. DETECT2000 and BUILDER V.6 for Simulation Studies

Monte Carlo simulations for determining both the optimal crystal material and the design features of the crystal array were performed using DETECT2000 and BUILDER Version 6 [2]–[5].

1) DETECT2000: DETECT2000 models the behavior of optical systems by isotropically generating individual scintillation photons in specified portions of the scintillator. The simulation follows each photon in its passage through the various components and interactions with surfaces, and records its fate (absorption, escape, or detection). Random samplings are made to determine if the photon is bulk absorbed, scattered, or wavelength shifted over this path. If none of these processes occur, the optical properties of the next surface determine whether the photon is reflected, refracted, detected, or absorbed. This process is then repeated for all subsequent paths in the history. Data of the fate of each photon are tabulated for all photons generated.

DETECT2000's definition statements define the optical properties of all materials and surface finishes that can be used in a simulation. The user specifies the materials, surface finishes, and geometries. Components such as crystal arrays and PMT glass windows can then be built out of these specifications.

2) Surface Definitions: The optical behavior of each surface is chosen by selecting one of the set of defined surface finishes. Surfaces may either be external (assumed to be an interface with a vacuum) or shared with another component. Surfaces in optical contact are treated using Snell's law of refraction

$$\frac{\sin(\theta_i')}{\sin(\theta_t')} = \frac{n_2}{n_1} \tag{1}$$

where n_1 and n_2 are, respectively, the refractive indexes of the first and second media at an interface, and θ_i' and θ_t' are, respectively, the angles of incidence and transmission with respect to the surface normal.

If the "POLISH" surface finish is chosen, a reflection coefficient may also be specified to represent an external diffuse reflector (e.g., $\mathrm{RC} = 0.98$). For surfaces that do not interface with another component, the value of the reflection coefficient determines the probability that a photon stays within the volume.

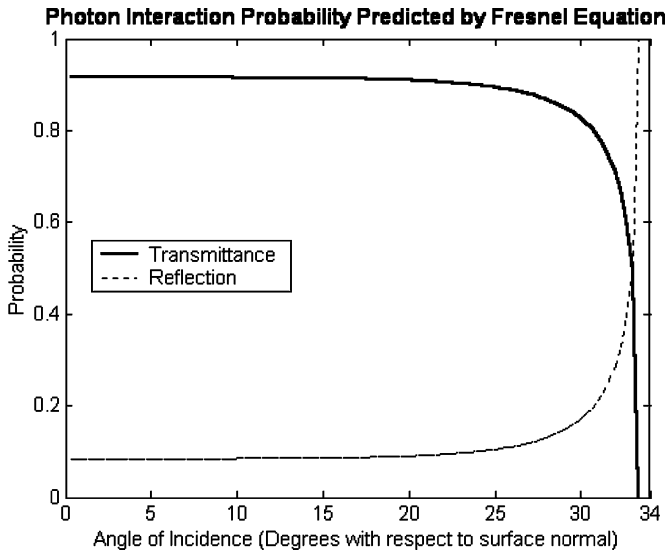

Fig. 1. Probability distributions of reflection (dashed curve) and transmittance (solid curve) for a photon traversing from index of refraction $\mathrm{n} = 1.82$ (LSO:Ce) to $\mathrm{n} = 1.0$ (vacuum).

Photons incident on surfaces are assumed to have random polarization. If a change in refractive index occurs at the surface between components, the following probability calculation is made based upon Fresnel reflection [2]

$$R = \frac{1}{2}\left[\frac{\sin^2(\theta_i' - \theta_t')}{\sin^2(\theta_i' + \theta_t')} + \frac{\tan^2(\theta_i' - \theta_t')}{\tan^2(\theta_i' + \theta_t')}\right] \tag{2}$$

where R is the probability of reflection, and θ_i' and θ_t' are, respectively, the angles of incidence and transmission with respect to a local normal of the surface. If reflection is selected, the angle of reflection is set equal to the angle of incidence. If reflection does not occur, the photon is transmitted with the complementary probability T

$$T = 1 - R \tag{3}$$

where R was the previous probability based on Fresnel's equation (2), and the photon is assumed to obey Snell's law of refraction. Fig. 1 illustrates (2) and (3) for one of the simulated crystal arrays in this paper. Depending on the refractive index change and the angle of incidence, this photon interaction may result in total internal reflection, or refraction of the photon through the surface and into the adjacent component.

A "GROUND" surface finish can be specified in order to simulate a roughened or ground optical surface. It is treated in the same way as the polished surface described earlier, except that the normal to the surface used in the refraction calculations is randomly distributed, following a Lambertian distribution (defined below), about the nominal surface normal.

The "PAINT" surface finish models a surface painted with a diffuse reflecting material characterized by user-defined reflection coefficients. If random sampling shows that reflection occurs, it is assumed to be Lambertian. In this case, the angle of reflection is independent of the angle of incidence, and is sampled from a distribution given by

$$I(\theta) = I_0 \cos(\theta) \tag{4}$$

TABLE I
RELEVANT PROPERTIES OF SCINTILLATION CRYSTALS USED IN LIGHT TRACKING SIMULATIONS

Scintillator	*Linear Attenuation Coefficient (cm^{-1})*	*Crystal Length for 93% Absorption 140 keV (mm)*	*Refractive Index*	*Approx. Light Yield 140 keV (photons)*	*Decay Time (ns)*
NaI(Tl)	2.61	10.0	1.85	4200	230
CsI(Tl)	3.85	7.5	1.79	4200	1000
CsI(Na)	3.85	7.5	1.79	3150	650
LSO(Ce)	9.74	3.0	1.82	3150	40
BGO	12.15	2.4	2.15	630	300
GSO(Ce)	6.68	4.4	1.91	1050	60

where $I(\theta)$ is the reflected intensity with respect to the surface normal and I_0 is the incident intensity.

The "DETECT" surface finish represents a photosensor (e.g., a photocathode or any other photon detecting layer of a photomultiplier tube). In the simulations presented here, the PMT was represented as a 2-mm-thick glass window with the bottom surface being the DETECT surface finish. Unless otherwise specified, every photon reaching the DETECT surface finish through the window is detected.

3) BUILDER Version 6.0: The BUILDER program simplifies the task of defining the geometrical properties of a model in DETECT by translating BUILDER's higher level component definition syntax into the language of DETECT [2]–[5]. For example, the user can define sophisticated scintillation detector designs by connecting simple box components with a block scintillator. Once each component has been defined, BUILDER connects them, checks for overlaps and incompatible surface finishes, and then translates these higher level definitions into the language of DETECT2000.

B. Simulation Studies

DETECT2000 and BUILDER V.6 were used to determine the optimal crystal material, crystal geometry, surface finishes, and the optimal coupling conditions for the Hamamatsu H8500 Position Sensitive Photomultiplier Tube (PSPMT) to be used in the gamma camera.

1) Optimizing Photon Output: Selecting LSO: In order to study light collection efficiency for different crystal materials and surface finishes, simulations of point light sources at different depths were performed within several crystal materials using the properties shown in Table I.

Each simulation varied in crystal material and surface finish. In each simulation, one crystal pixel was coupled to a glass window such that the bottom plane of the crystal was in contact with the top plane of the window. The centroid of the crystal was colinear with the centroid of the window.

Different surface finish types for each crystal material included polished, polished with reflector, ground, ground with reflector, and painted with reflector. For a crystal surface finish that included a reflector, the reflection coefficient used was

$\mathrm{RC} = 0.98$. For each crystal, the top plane used a PAINT, $\mathrm{RC} = 0.98$ finish, and the bottom plane used a POLISH finish.

Each crystal was coupled to a $52\ \mathrm{mm} \times 52\ \mathrm{mm} \times 2\ \mathrm{mm}$ glass window. Its index of refraction was specified as 1.5. The surfaces of the PMT glass window used a POLISH finish with its bottom surface being the DETECT finish.

Within each crystal, 5000 photons, representing one scintillation event, were generated at three points within the volume of the pixel: 0.05 mm below the top of the crystal, in the middle of the crystal, and 0.05 mm above the bottom of the crystal. The absolute number of photons collected, per crystal and surface finish, was calculated using the mean number of light photons collected from these simulated point source depths, which were each weighted by the interaction probability at that given depth.

Criteria for selecting the appropriate crystal material included light output and peak emission wavelengths compatible with the peak absorption wavelength of the Hamamatsu H8500 Position Sensitive Photomultiplier Tube (PSPMT)

2) Measured $^{176}\mathrm{Lu}$ *Background Rate in LSO Array:* LSO was chosen based on the results as detailed in the "Results and Discussion" section. In order to determine whether or not the background activity of LSO would be problematic for the proposed miniature gamma ray camera, the $^{176}\mathrm{Lu}$ background rate of LSO was measured for a 23×23 array of $2\ \mathrm{mm} \times 2\ \mathrm{mm} \times 3\ \mathrm{mm}$ LSO crystals coupled to a Hamamatsu H8500 Flat-Panel PSPMT.

The total background rate was measured using an open energy window and a 20% window at about 122 keV.

3) Light Distribution Linearity: Continuous Crystal versus Discrete Crystal Array: Simulations were performed for 6 cm $\times$ 6 cm LSO(Ce) continuous sheets with a polished finish, which were also compared to simulations of 6 cm $\times$ 6 cm NaI(Tl) continuous sheets with a polished finish.

Simulations were also performed for arrays of 20×20 discrete $2\ \mathrm{mm} \times 2\ \mathrm{mm} \times 3\ \mathrm{mm}$ crystals which were separated by fixed air gaps and with different finishes including polished with reflector $(\mathrm{RC} = 0.98)$, ground with reflector $(\mathrm{RC} = 0.98)$, and ground without reflector. For both crystal sheets and arrays, the top and perimeter surfaces used a ground with reflector $(\mathrm{RC} = 0.98)$ finish.

Per scintillation event, 5000 photons were generated. The source position was moved across the crystal horizontally, from the center (in x-y and at average interaction depth) toward the edge, and data was collected to compare the linearity of the collected light photons in continuous sheets versus discrete crystal arrays.

4) Light Distribution Width for Crystal Array: Simulations were performed for arrays of 20×20 LSO(Ce) discrete crystal with varying properties. The arrays were coupled to optical coupling grease, which in turn was coupled to a glass window. Per crystal array, its optical grease and glass window had the same length and width as the array.

Simulated array properties included all possible combinations of ground crystals, with and without reflector, and with and without optical coupling grease. For arrays with reflectors, air gaps between discrete crystals were 0.2 mm, while arrays without reflectors had 0.01 mm air gaps between discrete crystals. For all arrays, the top and perimeter surfaces used a ground with reflector finish, while the bottom surface used a polish finish.

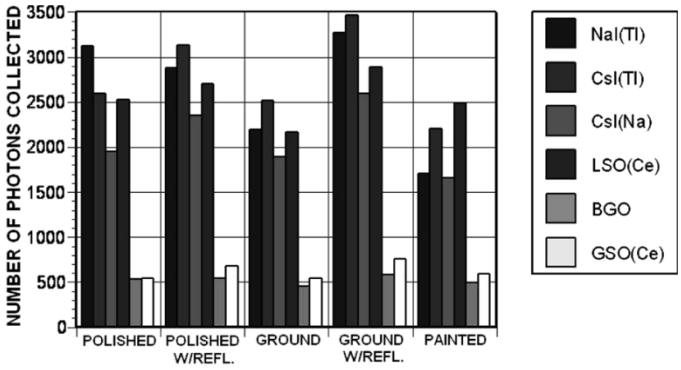

Fig. 2. Absolute number of photons collected from 2 mm $\times$ 2 mm cross-section crystals of different materials and surface conditions ("REFL:"= white reflector) using parameters given in Table I.

The optical coupling grease was simulated as 0.01 mm thick. Its index of refraction was specified as 1.465 [8]. All of its surfaces used polished finish.

The glass window was simulated as 2 mm thick. Its index of refraction was specified as 1.5. Its bottom surface was the DETECT surface, while its other surfaces used polished finish.

Per crystal array, 5000 photons were simulated to represent one event. The source was located in the center crystal of the array and 0.05 mm below the top of the crystal.

Data was obtained of the number of collected light photons and distribution width of the detected photons as seen by the PMT surface.

C. Experimental Measurements

In order to validate the results of these simulations, physical experiments were performed by flood irradiating a 5×5 array of $2\ \mathrm{mm} \times 2\ \mathrm{mm} \times 3\ \mathrm{mm}$ LSO(Ce) crystals with a $^{57}\mathrm{Co}$ source (122 keV). For all cases the outer array boundaries were wrapped in five layers of Teflon tape. The Teflon tape was $\sim$0.15 mm thick between crystals and $\sim$0.25 mm thick on top and sides of the array. The setup utilized a charge multiplexed readout of a Hamamatsu H8500 PSPMT [7].

III. Results and Discussion

A. Optimizing Photon Output: Selecting LSO

Using the properties of Table I, results from simulations of the varying crystal materials and surface finishes are graphed in Fig. 2. Note that although CsI(Tl) appears to collect the most photons, its emission peak wavelength is 580 nm, which is not a good spectral match to the absorption spectrum of the H8500 PSPMT (peak absorption at 420 nm for a bialkali photocathode), and will result in a significantly lower quantum efficiency [6].

The next highest absolute light collection is from NaI(Tl). However, this crystal material is hygroscopic, and thus requires a hermetically sealed package, which can be expensive, especially for crystal arrays.

The crystal material with the next highest light output into the PMT is LSO(Ce). A noteworthy feature of LSO(Ce) is that due to its high effective Z (66) and density ($7.4\ \mathrm{g/cm^3}$), just 3-mm-thick LSO is required for 95% detection efficiency of 140-keV

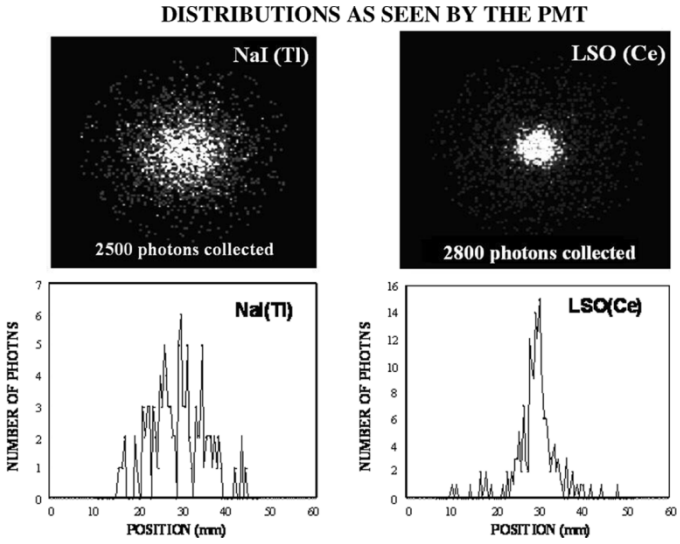

Fig. 3. Results from simulations of 5000 photons generated at the center of 6 cm × 6 cm crystal sheets, and at their respective average depths of interaction. **Top Left**: NaI(Tl) sheet, 10 mm thick; **Top Right**: LSO(Ce) sheet, 3.5 mm thick. **Bottom**: profiles through the distributions.

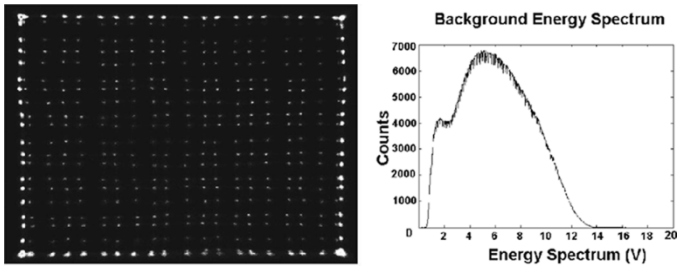

Fig. 4. **Left**: background events for the LSO array. Multiple rows of crystals on the same anode row at PSPMT edges produce the hot perimeter artifact. **Right**: energy spectrum shows well-known characteristics of a beta emitter. 14 V corresponds to approximately 1193 keV, which is the ^{176}Lu beta spectrum endpoint energy.

photons. A benefit of thin crystal dimensions is improved light collection and narrow light spread. Fig. 3 illustrates that because LSO can be thinner for the same stopping power as 10-mm-thick NaI(Tl), for sheet configurations, the light distribution is narrower and absolute light collected is greater for LSO, which will yield better intrinsic spatial and energy resolutions.

Even though NaI(Tl) has been the standard scintillation crystal for gamma cameras, and although LSO is normally used in positron emission tomography (PET), these results strongly suggested that LSO:Ce would be the best choice for the gamma camera [1].

B. Measured ^{176}Lu *Background Rate in LSO Array*

Fig. 4 shows approximately 2.6 million background events of ^{176}Lu measured from a 23 × 23 array of 2 mm × 2 mm × 3 mm LSO crystals coupled to a Hamamatsu H8500 Flat-Panel PSPMT.

The measured total background rate (room+^{176}Lu) using an open energy window was ∼ 63 cps/cm^3, or ∼0.76 counts per second (cps) per crystal, which is low since the volume of each 2 mm × 2 mm × 3 mm LSO crystal is only 0.012 cm^3. LSO background rates were measured to be approximately 1.6 cps/cm^3 in a 20% window at about 122 keV, which for

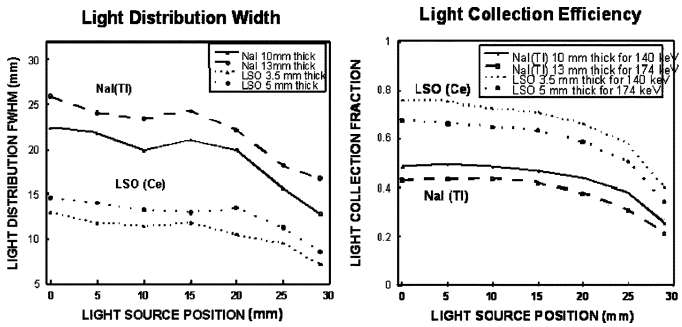

Fig. 5. **Left**: FWHM of the light distributions as a function of light source position for 10- and 13-mm-thick NaI(Tl) and 3.5- and 5-mm-thick LSO crystal sheets (6 cm × 6 cm area, no entrance window). The different crystal thickness correspond to >95% absorption efficiency for 140- and 170-keV photons, respectively. Light distribution widths were extracted from fits to a Lorentzian distribution. **Right**: Fraction of light collected as a function of source position across the face of the crystal. The origin is at the center of the crystal, and at the average interaction depth.

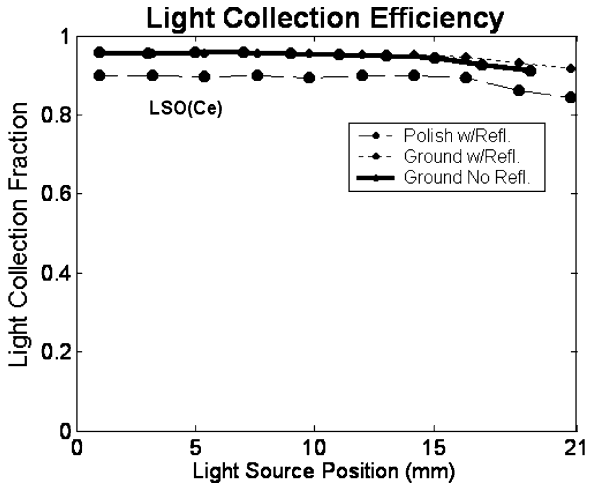

Fig. 6: Light collection versus light source position (mm) from center to one edge for LSO(Ce) with three different array properties: polished crystals with intercrystal reflectors (RC = 0.98), ground crystals with intercrystal reflectors (RC = 0.98), and ground crystals without intercrystal reflectors. Please note that the plot for the ground crystals ends before the other two arrays due to the lack of intercrystal reflectors. 5000 photons were simulated to represent one scintillation event, which occurred 0.05 mm below the top of the crystal. Mean number of light photons collected per source position are plotted here.

a 5 cm × 5 cm × 0.3 cm crystal volume translates into a background rate of only 12 cps over the entire 5 cm × 5 cm FOV or 0.02 cps per LSO crystal.

C. Light Distribution Linearity: Continuous Crystal Versus Discrete Crystal Array

Fig. 5 illustrates that for a 3.5-mm-thick continuous LSO sheet, light collection efficiency is higher and the light distributions are narrower than for a 10-mm-thick continuous NaI(Tl) sheet.

As seen in Fig. 5, however, the light distribution nonlinearities in crystal sheets will be problematic for a small 5 cm × 5 cm FOV camera. As a result, light distribution linearity for an array of discrete crystals was investigated.

Fig. 6 plots the number of light photons collected as a function of position of a point source. All three plots here represent simulations of 20 × 20 arrays of 2 mm×2 mm×3 mm LSO crystals, with 10 μm optical coupling grease (n = 1.465) between the

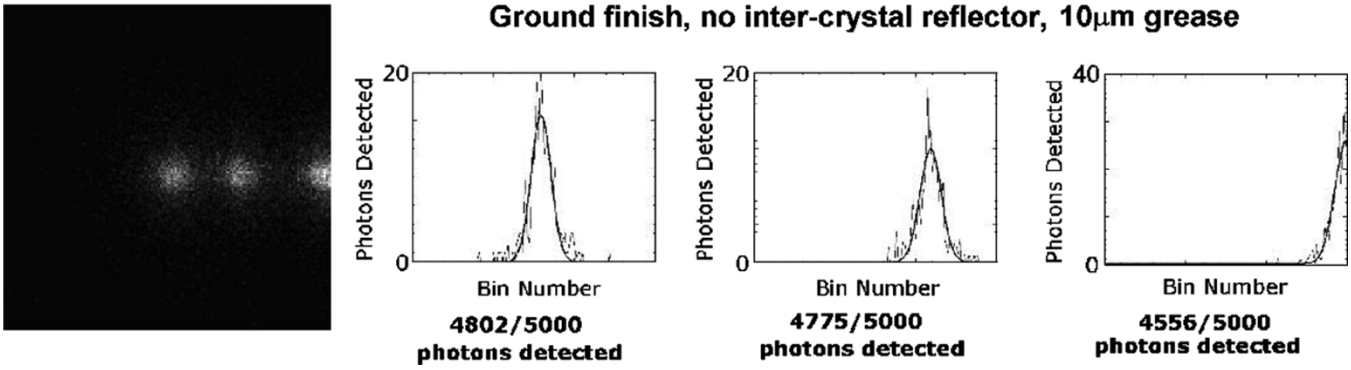

Fig. 7. These distributions correspond to moving a source across the face of a 20 × 20 array of ground LSO crystals with no intercrystal reflector.

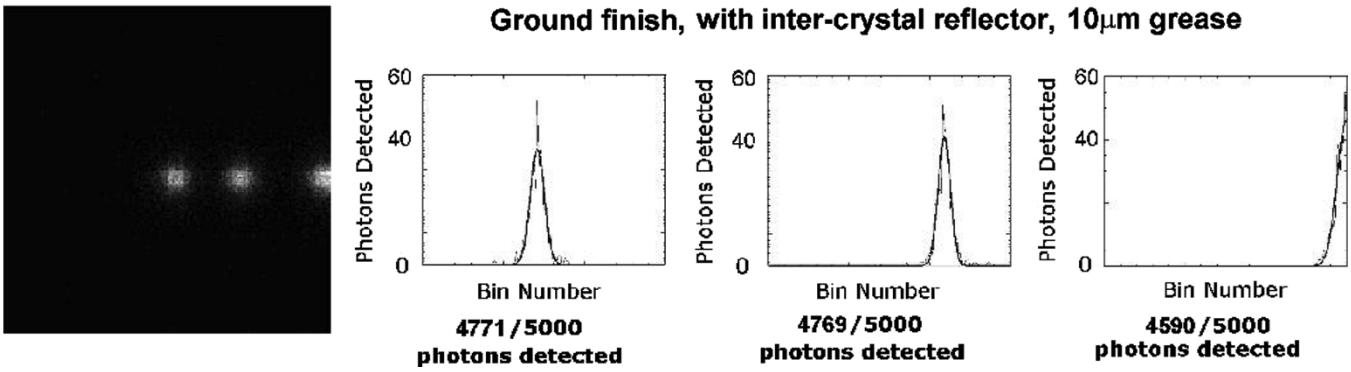

Fig. 8. These distributions correspond to moving a source across the face of a 20 × 20 array of ground LSO crystals with intercrystal reflector.

array and PSPMT glass window (2 mm thick, $\mathrm{n} = 1.5$), and reflector $(\mathrm{RC} = 0.98)$ on the top and perimeter of the array block.

Each point represents one scintillation event, which was simulated with 5000 photons generated 0.05 mm below the top of the crystal. Generating the photons in other locations within the crystal volume of this discrete crystal array would produce similar relatively linear trends to that observed in Fig. 6.

As seen in Fig. 6, simulations of these discrete crystal arrays exhibit improved light distribution linearity compared to continuous crystals (Fig. 5) independent of surface conditions and reflectors. This improvement is due to the isolation of the individual crystal pixels and improved light focusing onto the photodetector.

D. Light Distribution Width for Crystal Array

Figs. 7 and 8 show light distributions as seen by the PSPMT for 5000 simulated light photons and their corresponding profiles through the center of the distributions. The arrays were arrays of 20×20 ground $2\,\mathrm{mm} \times 2\,\mathrm{mm} \times 3\,\mathrm{mm}$ LSO crystals without and with intercrystal reflector, for Figs. 7 and 8, respectively. For both cases, reflector was used on the perimeter and top of the array block, and a 0.01-mm-thick layer of grease is coupled between the array block and the 2-mm-thick PSPMT glass window. The reflection coefficients of the reflectors specified here and in subsequent simulations are $\mathrm{RC} = 0.98$. Note that for each light distribution image, the three distributions shown were generated separately and then summed. These figures also illustrate the linearity discussed in the previous section.

Results from further studies using an increased grease thickness and different crystal conditions are shown in Figs. 9 and 10. Note that in Fig. 9 (Left) the conditions of no intercrystal reflector and coupling grease between the array and PSPMT tend to increase light diffusion onto the PSPMT face, while the conditions of intercrystal reflector and no grease in Fig. 10 (Right) tend to improve the light focusing onto the PSPMT. Thus, the overall narrowest light distribution case is that which has intercrystal reflector and no coupling grease (Fig. 10, right). A narrow light distribution is desirable for high spatial resolution, however adequate light diffusion is necessary to spread the light among the 8×8 array 5.6 mm × 5.6 mm PSPMT anodes for uniform and linear positioning.

It is interesting to note from Figs. 9 and 10 that the use of coupling grease for crystals with or without intercrystal reflector tends to diffuse light to a greater extent than not using coupling grease with only ∼6% better overall light transmission into the PMT. Thin (10 $\mu\mathrm{m}$) or thick 200 $\mu\mathrm{m}$) grease produced similar light collection and distribution results (see Fig. 11).

One may use Snell's Law (1) and Fresnel reflection (2) to explain the result that the simulated arrays with coupling grease diffuse more light onto the PMT than the arrays without coupling grease (Note: For the nongreased case, a 100-$\mu\mathrm{m}$ layer of air with $\mathrm{n} = 1.0$ was used between the crystal array and the PMT window). Equations (1)to (3) can be used to deduce that only those photons that approach an interface with angles between 0 and $\arcsin(n_2/n_1)$ will satisfy the domain of the arcsin function in the calculations of the reflection and transmission probabilities. That is, as long as a photon approaches the interface in certain angular ranges, there will be a nonzero probability that it will transmit and ultimately be detected by the PMT. For example, a photon traversing from LSO $(n_1 = 1.82)$ to

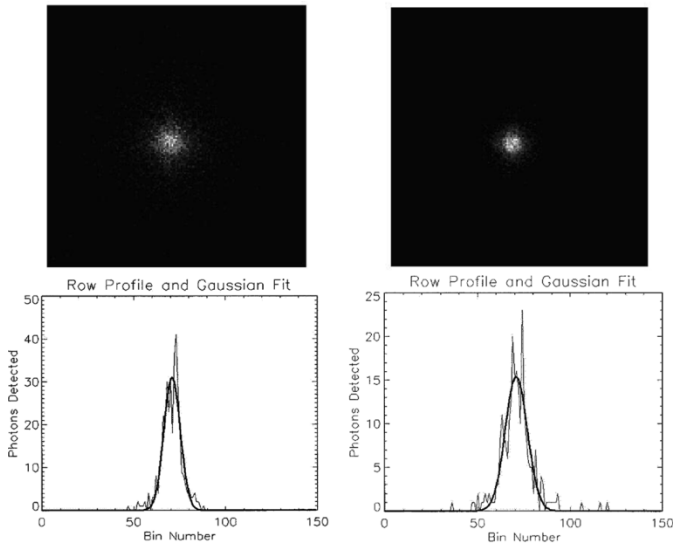

Fig. 9. **Left**: Ground crystals, no reflector, with (200 μm thick) coupling grease. 4800/5000 photons were collected. **Right**: Ground, with reflector, with (200 μm thick) grease. 4786/5000 photons were collected.

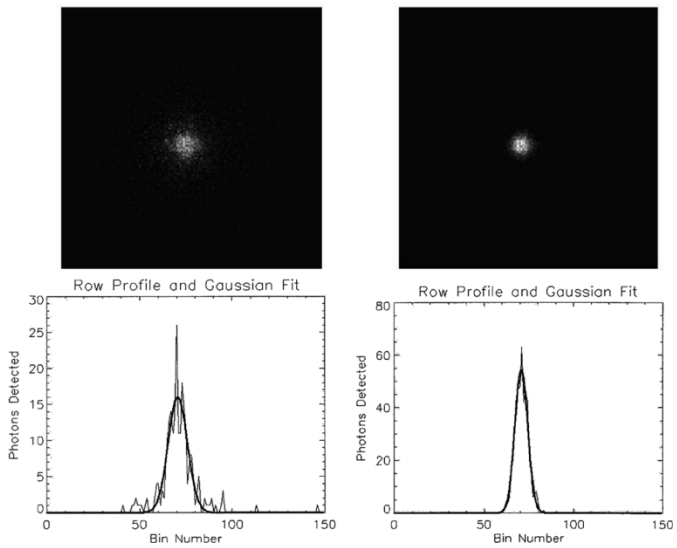

Fig. 10. **Left**: Ground crystals, no reflector, no grease. 4510/5000 photons were collected. **Right**: Ground crystals, with reflector, no grease. 4518/5000 photons were collected.

the coupling grease $(n_2 = 1.465)$ may be transmitted if it approaches the interface with angles between 0° and 54°. On the other hand, the entrance angles that promote transmission for a photon entering air $(n_2 = 1.0)$ from LSO are 0° and 33°. Thus, for the nongreased case, essentially only forward directed photons will be detected.

Furthermore, the changes of index of refraction explain the differences in light distribution FWHM for the arrays with and without grease. In the array with grease, photons that were able to transmit from LSO to the grease $(\mathrm{n} = 1.465)$ must then traverse through the 2-mm-thick glass $(\mathrm{n} = 1.5)$ entrance window of the simulated PMT in order to be detected. Since these indices of refraction are quite similar, the photons that transmit from the grease to the glass will very nearly continue along their initial path and be detected. Thus, the distribution of photons detected on the PMT photocathode surface will be very similar in shape

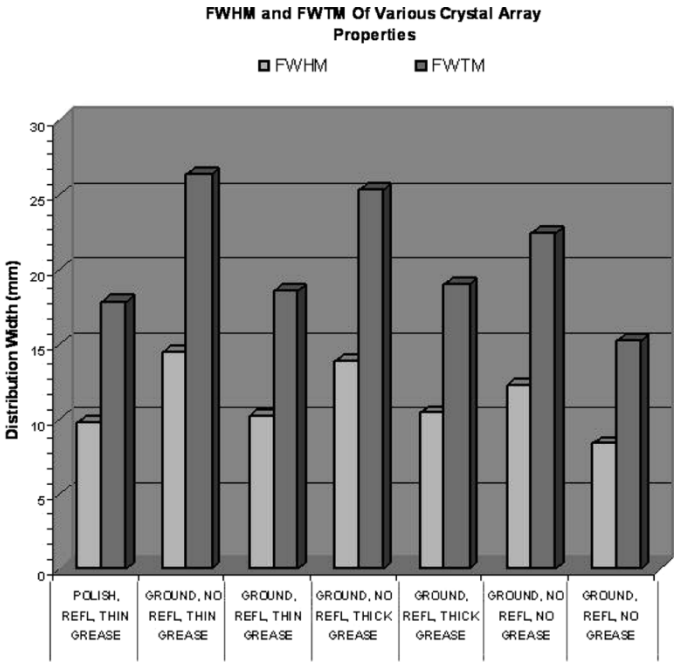

Fig. 11. FWHM and FWTM for all discrete crystal array simulations.

but slightly magnified in the PMT glass window compared to the distribution that would be presented at the grease-glass interface. On the other hand, for the array coupled to the PMT without grease, photons must traverse from air $(\mathrm{n} = 1.0)$ to the PMT window $(\mathrm{n} = 1.5)$. Therefore, the net effect of this increase in the index of refraction causes the photons to bend more toward the normal to the surface. The distribution of photons, then, will be compressed and the FWHM will be narrower, as seen in Fig. 11.

Both the FWHM and FWTM for all of these simulations are summarized in Fig. 11.

E. Experimental Measurements

Experiments were performed by flood irradiating a 5×5 array of $2\ \mathrm{mm} \times 2\ \mathrm{mm} \times 3\ \mathrm{mm}$ LSO(Ce) crystals with a $^{57}\mathrm{Co}$ source (122 keV). For all cases the outer array boundaries were wrapped in five layers of Teflon tape. The setup utilized a charge multiplexed readout of a Hamamatsu H8500 PSPMT [7]. Each of the images shown in Fig. 12 represents ~780 000 counts.

The crystal flood images are consistent with the simulation results of light distributions. In general, arrays without grease (Fig. 12, top) tend to focus light more than arrays with grease (Fig. 12, bottom).

The conditions of no intercrystal reflector and no optical coupling grease (Fig. 12, top left) represents an interplay between the light focusing effect of the no grease case and the spreading nature of the no reflector condition. Too much light spread (~12 mm FWHM from Fig. 11) results from this condition, which explains why the crystals are not as well distinguished.

The conditions of intercrystal reflector and coupling grease (Fig. 12, bottom right) has a more appropriate balance between the focusing and spreading effects (~9 mm FWHM from Fig. 11) for the 6 mm PSPMT anode pitch, resulting in improved crystal delineation. For this latter condition there

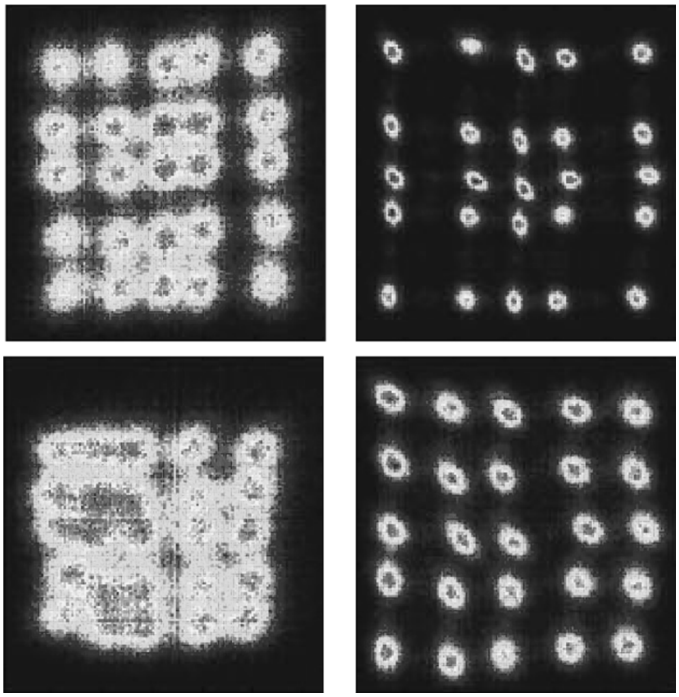

Fig. 12. The four event position histogram images each represent approximately a 780 000 count raw flood $^{57}\mathrm{Co}$ irradiation of a 5 × 5 array of 2 mm × 2 mm × 3 mm LSO(Ce) crystals placed at an identical location near the edge of a Hamamatsu H8500 PSPMT. No energy gating was used in a photosensitive window from 50–300 keV. **Left column**: Ground, without reflector. **Right column**: Ground, with reflector. **Top row**: Without grease. **Bottom row**: With grease.

is relatively poor light diffusion presented at the LSO-grease interface due to the intercrystal reflectors, and most of the light spread occurs within the grease and PMT glass entrance window.

The conditions of with reflector, no grease (Fig. 12, top right) exhibit the greatest light focusing, but inadequate light diffusion (∼6 mm FWHM from Fig. 11) for positioning with the 6 mm PSPMT anode pitch.

As seen in Fig. 12 (bottom left), the ground, no reflector, with grease case exhibits overdiffusion of light (∼14 mm FWHM from Fig. 11) and the individual crystals are not well resolved.

IV. Summary and Conclusion

Objectives in designing the scintillation crystal array for the proposed miniature gamma ray camera include optimizing light collection, spatial linearity, and spatial resolution for the particular PSPMT anode configuration that will be used.

In comparison to other types of scintillation crystals, LSO(Ce) was investigated because of (1) its compatibility with the absorption spectrum of a PMT photocathode, (2) its high stopping power at 140 keV (just a 3-mm thickness is required), and (3) its low cost compared to hermetically sealed pixilated NaI(Tl) arrays. Since a low volume of LSO required, the background rate is also low (∼0.02 cps per 2 mm × 2 mm × 3 mm LSO crystal in a 20% window around 122 keV).

For the proposed lymph node application, the entire 5 cm × 5 cm FOV of the gamma camera must be sensitive. Therefore, the spatial and spectral nonlinearities in sheet crystals can be problematic. An array of discrete crystals was chosen because they exhibit better spatial linearity, which causes the camera response to be more uniform and linear toward the edge of the FOV.

Simulation studies have shown that the ground finish, *without* intercrystal reflector, *with* optical coupling grease conditions tend to spread the light more onto the PSPMT than do the ground finish, *with* intercrystal reflector, *without* optical coupling grease crystal arrays. Although the latter conditions improve light focusing, more light diffusion would be necessary for adequately spreading light among the 5.6 mm × 5.6 mm PSPMT anodes (6 mm pitch) for accurate and linear positioning.

Experimental data from the $^{57}\mathrm{Co}$ flood images are consistent with simulation results of light distributions. The conditions *without* intercrystal reflector (Fig. 12, left) tend to diffuse the light to a greater extent than the conditions *with* intercrystal reflector (Fig. 12, right), which explains why the crystals are not as well distinguished. In this left column of Fig. 12, however, the condition *without* coupling grease (Fig. 12, top left) delineates the crystals better than the condition *with* coupling grease (Fig. 12, bottom left).

The conditions *with* intercrystal reflector (Fig. 12, right) tend to focus the light to a greater extent than the conditions *without* intercrystal reflector (Fig. 12, left). In this right column of Fig. 12, however, the condition *without* coupling grease (Fig. 12, top right) tends to focus the light too much. On the other hand, the condition *with* coupling grease constrains the light exiting the crystals, while also optimizing light collection (Fig. 12, bottom right). Due to the combination of the coupling grease and the 2-mm-thick PMT entrance window, this latter condition provides a more appropriate light spread over the 6 mm pitch PSPMT anodes to better delineate the crystals (Fig. 12, bottom right).

References

[1] C. S. Levin, "Detector design issues for compact nuclear emission cameras dedicated to breast imaging," *Nucl. Instrum. Methods in Physics Res.*, vol. A 497, pp. 60–74, 2003.

[2] C. Moisan, F. Cayouet, and G. McDonald, *DETECT2000: The Object Oriented C++ Language Version of DETECT: A Program for Modeling Optical Properties of Scintillators*. Quebec City, Quebec, Canada: Dep. Elect. Comput. Eng. Laval University.

[3] *http://www.gel.ulaval.ca/detect/* [Online]

[4] C. Moisan and G. McDonald, *BUILDER: A High Level Language Interface to DETECT for the Design of Scintillation Detectors: User's Manual, Version 6.0*. Quebec City, Quebec, Canada: Dep. Elect. Comput. Eng. Laval University.

[5] *http://www.gel.ulaval.ca/detect/* [Online]

[6] C. Moisan, F. Cayouet, and G. McDonald, *DETECT2000, Version 5.0*, Sep. 1, 2000.

[7] *http://www.gel.ulaval.ca/detect/* [Online]

[8] C. Moisan and G. McDonald, *BUILDER Ver6.0*, Sep. 2000.

[9] *http://www.gel.ulaval.ca/detect/* [Online]

[10] *http://usa.hamamatsu.com/* [Online]

[11] P. D. Olcott, J. A. Talcott, C. S. Levin, F. Habte, and A. M. Foudray, "Compact readout electronics for hand-held gamma ray imagers," in *2003 IEEE Medical Imaging Conf.*.

[12] Silicone Optical Grease*http://www.bicrondirect.com/sili.htm* [Online]

[13] C. S. Levin, E. J. Hoffman, M. P. Tornai, and L. R. MacDonald, "PSPMT and photodiode designs of a small scintillation camera for imaging malignant breast tumors," *IEEE Trans. Nucl. Sci.*, vol. 44, no. 4, pp. 1513–1520, Aug. 1997.

[14] L. R. MacDonald, B. E. Patt, and J. S. Iwanczyk *et al.*, "High-resolution hand-held gamma camera," in *2000 SPIE Medical Applications of Penetrating Radiation Conference*, San Diego, CA, Aug. 2000.

[15] C. S. Levin, E. J. Hoffman, M. P. Tornai, and L. R. MacDonald, "Design of a small scintillation camera with photodiode readout for imaging malignant breast tumors," *J. Nucl. Med.*, vol. 37, p. 52, May 1996.

[16] C. S. Levin, E. J. Hoffman, R. W. Silverman, A. K. Meadors, and M. P. Tornai, "Breast tumor detectability with small scintillation cameras," in *1997 IEEE Medical Imaging Conf.*, NM.

[17] A. J. Soares, I. Cullum, D. J. Miller, G. J. Royle, and R. D. Speller, "Development of a small gamma camera using wavelength-shifting fibers coupled to inorganic scintillation crystals for imaging 140 keV gamma rays," *IEEE Trans. Nucl. Sci.*, vol. 46, no. 3, pp. 576–582, Jun. 1999.

[18] C. E. Ordonez, R. A. Mintzer, S. N. Aarsvold, N. J. Yasillo, and K. L. Matthews, "Simulation of imaging with sodium iodide crystals and position-sensitive photomultiplier tubes," *IEEE Trans. Nucl. Sci.*, vol. 41, no. 4, pp. 1510–1515, Aug. 1994.

[19] H. Watabe, T. Nakamura, H. Takahashi, M. Itoh, M. Matsumoto, and A. Yamadera, "Development of a miniature gamma-ray endoscopic probe for tumor localization in nuclear medicine," *IEEE Trans. Nucl. Sci.*, vol. 40, no. 2, pp. 88–94, Apr. 1993.

[20] J.-H. Kim, Y. Choi, K.-S. Joo, B.-S. Sihn, J.-W. Chong, and S. E. Kim *et al.*, "Development of a miniature scintillation camera using an NaI(Tl) scintillator and PSPMT for scintimammography," *Phys. Med. Biol.*, vol. 45, pp. 3481–3488, 2000.